

PHOTOACTIVITY OF HEMATITE ELECTRODE PREPARED VIA ANODIC ELECTRODEPOSITION ON FTO AND FTO/TiO₂ SUBSTRATES

M. SIMA^{a*}, E. VASILE^b, MA. SIMA^a

^aNational Institute of Materials Physics, No.405A Atomistilor Street, 077125 Magurele, Romania

^bUniversity "Politehnica" of Bucharest, Faculty of Applied Chemistry and Material Science, Department of Oxide Materials and Nanomaterials, No. 1-7 Gh. Polizu Street, 011061 Bucharest, Romania

The hematite films were prepared via anodic electrodeposition on FTO and FTO/mesoporous TiO₂ substrates. The hematite photoanodes were characterized by X-ray diffraction and scanning electron microscopy. The performance of the prepared hematite photoanodes was assessed based on photocurrent-voltage curves and electrochemical impedance spectra. The modification of the hematite surface with nickel oxide nanoparticles improved the performance of the hematite photoanode while phosphorous doped hematite photoanode shows poor photoactivity. The onset of water oxidation photocurrent was cathodically shifted for hematite photoanodes prepared on FTO/TiO₂ substrate.

(Received May 29, 2017; Accepted August 1, 2017)

Keywords: Water splitting, Pristine and doped hematite, Mesoporous TiO₂, Nickel oxide

1. Introduction

Electrolytic decomposition of water with hydrogen (H₂) and oxygen (O₂) generation is an electrochemical process that uses electrical energy as the driving force of chemical reactions. To achieve a current density of 1A/cm², a normal value for water electrolysis, a cell voltage of 1.85-2.05 V is required due to overpotentials at both cathode and anode. Considering the values of thermodynamic potential necessary for water splitting in H₂ and O₂ (1.23 V) and of electrolysis potential (1.85-2.05 V) then energy efficiency of electrolysis has the upper limit 60-66.5%, with an energy loss of 33.5-40% [1]. In addition, the electrolyzers are expensive. Consequently, only 4% of the hydrogen produced in the world is obtained by water electrolysis [2].

Starting with the studies of Fujishima and Honda on semiconductor electrodes [3], the use of solar energy for water splitting was considered. These studies were the basis of technology of photoelectrochemical cell (PEC) for water splitting. Water splitting by a photoelectrochemical route offers promising perspectives for both sustainable energy generation and energy storing as hydrogen. Therefore, fabrication of efficient photoelectrochemical cells for water splitting and the production of storable hydrogen is a very active research direction. The PEC cell contains a photoelectrode that absorbs light and a counter electrode, both immersed in an aqueous solution. The main component of the PEC cell is a semiconductor that converts incident photons into electron-hole pairs when is exposed to sunlight. An ideal semiconductor for water photolysis must have high chemical stability in water, low production costs, good absorption of visible light, good transport of electric charges and catalytic capacities. Also, the energy range between the edges of the valence and conduction bands of the semiconductor must include the potentials both of reduction and oxidation of water. Despite of many research efforts, such a semiconductor has not been found.

* Corresponding author: msima@infim.ro

Hematite ($\alpha\text{-Fe}_2\text{O}_3$) is one of the most promising materials for water splitting. This material is a n-type semiconductor with a band gap of 2.1-2.2eV [4-7], is stable, abundant and non-aggressive in the environment, its band gap allows the absorption of a good part of the solar spectrum ($<620\text{nm}$) and has the valence band edge position suitable for water oxidation [8-10]. However, this material has a diffusion length of minor carriers reduced to only 2-4nm [8] or 20nm [9] and possesses a slow kinetics for the transfer of holes to water molecules [10]. Additionally, absorption is reduced near the absorption edge due to its indirect band gap, with a photon penetration length of $\sim 0.1\text{-}1\ \mu\text{m}$ at 500-600nm [11, 12], which is significantly greater than the length of the hole diffusion. Therefore, the holes generated away from the surface will recombine before reaching the semiconductor/liquid interface. On the other hand, the conduction band of the hematite has an inadequate position for water reduction process. As a result it is necessary to apply an external bias to generate hydrogen at counter electrode and this can be supplied by a tandem cell [13-15]. The ideal PEC system should work without an external applied voltage, and for this, combinations of two or more semiconductors can be made. For example, the photoanode can be used in a tandem arrangement with a photocathode or a photovoltaic cell. Titania (TiO_2), a semiconductor with a wide band gap (3.2 eV) and natural n-type electrical conductivity has been the first material tested for photoelectrochemical splitting of water [3]. The major drawback of TiO_2 in its use in photoelectrochemical cells is its wide bandgap. To improve the photocatalytic activity of TiO_2 has been changed its active surface with a semiconductor with small band gap [16].

In this paper, hematite thin films are prepared by electrodeposition on FTO (F:SnO_2) and FTO/ TiO_2 substrates. The influences of the substrate, doping phosphorous into hematite structure and surface treatment with nickel oxide on photoelectrochemical performances of the hematite films were studied.

2. Experimental section

The hematite films were synthesized on FTO (F:SnO_2) and FTO/ TiO_2 substrates by electrochemical and annealing processes. The electrodeposition process was performed potentiostatically at 1.2V for 2200s in a conventional three-electrode cell configuration at room temperature using as electrolyte an aqueous solution of 0.1M FeSO_4 . The electrochemical cell also contains a platinum foil as an auxiliary electrode and an Ag/AgCl electrode in saturated KCl as a reference electrode. The electrochemical processes were performed using an Autolab PGSTAT 30 potentiostat digitally controlled by a computer. Mesoporous TiO_2 layers were deposited on FTO substrate by spin-coating TiO_2 paste (Dysol 18NR-T) diluted further in ethanol absolute at 1:3 by weight at 2000 rpm for 60 s. The layers were then annealed at 550°C for 1h. The precursor for the synthesis of NiO [17] nanoparticles was prepared with 0.065 g nickel formate dihydrate in 6 ml ethylene glycol solution containing 26 μl ethylenediamine and filtered with 0.45 μm PTFE filters. This solution was sprayed on the substrate heated at 275°C . The distance between the spray nozzle and the substrate was 10 cm and the spray pressure 5 psi. The microstructures of deposits were imaged by field emission scanning electron microscopy (FESEM), using FEY Quanta Inspect scanning electron microscopes. X-ray diffraction (XRD) analyses were performed on a Bruker D8 Advance type X-ray diffractometer, in focusing geometry, equipped with copper target X-ray tube and LynxEye one-dimensional detector. The photoelectrochemical measurements were carried out in 1M NaOH electrolyte with a three-electrode electrochemical system composed of the hematite films as the working electrode, Ag/AgCl /saturated KCl as reference electrode, and a Pt foil as the counter electrode. The photoanodes were illuminated from the front side using AM1.5 solar simulator (L.O.T.-Oriol GmbH & Co.KG, Model LS0306 with a 300 W Xe-Arc lamp and an AM1.5-Global filter (LSZ189) with the specification: 1sun at 18 cm working distance). The polarization curves were measured in the dark and under illumination with a scan rate of 20mV/s. These measurements were conducted using a potentiostat/galvanostat Autolab PGSTAT 30 (Eco Chemie). The electrochemical impedance spectroscopy (EIS) spectra were collected in a frequency range of 100 KHz to 0.1 Hz with amplitude of 10 mV. The obtained curves were fitted using a Zview software.

3. Results and discussion

The hematite film was prepared by an electrochemical process of deposition of iron oxyhydroxide (FeOOH) film followed by an annealing process.

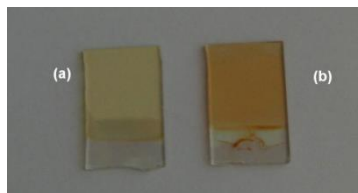


Fig.1. Photo images of iron oxyhydroxide (a) and hematite (b) films deposited on FTO substrate

The deposition of FeOOH film from a solution 0.1M FeSO₄ at anodic potential takes place in two steps which include oxidation of Fe²⁺ ions to Fe³⁺ ions, in a first step and precipitation of the of Fe³⁺ ions as iron oxyhydroxide, in a second step [18]. The as deposited film on FTO substrate is amorphous and shows uniform yellow color (Fig.1a). This film annealed for two hours at 525^oC exhibits an orange-red color (Fig.1b) and becomes crystalline, as a result of FeOOH film conversion into hematite (α -Fe₂O₃) film. In order to remove all hydroxyls from hematite it is necessary annealing over 800^oC [19]. This sintering process called “activation of hematite” increases the performance of the hematite as photoelectrode in photoelectrochemical cell [20]. At such temperatures FTO substrate could be deteriorated. Therefore, the hematite film was further annealed at 800^oC for only 10 min.

The hematite films annealed at 525^oC and 800^oC exhibited typical diffraction peaks (Fig.2) assigned to crystalline hematite planes (012), (104), (110), (113), (024) and (300) according to the ICDD PDF 04-015-9903

Fig.3a shows a SEM image of hematite thin film formed on the bare FTO substrate. This film has a nanostructured morphology composed of nanoparticles of about 40 nm that are tightly united.

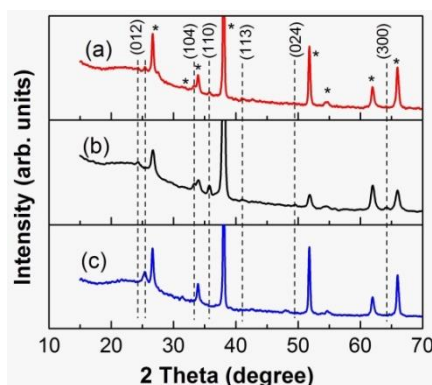


Fig.2. Diffractograms of hematite films deposited on (a) FTO/TiO₂ and (b) FTO substrates; (c) TiO₂ mesoporous film . * Indicates peaks attributed to the FTO substrate

In another experiment, hematite film was deposited on FTO/mesoporous TiO₂ substrate. XRD patterns of hematite film deposited on this substrate and of hematite and mesoporous TiO₂ films deposited separately on FTO substrate are presented in the Fig.2. It can be observed (Fig.2a) that XRD pattern of the structure FTO/TiO₂/hematite shows both the peaks of hematite and TiO₂ anatase phases.

The hematite film deposited on FTO/mesoporous TiO₂ substrate (Fig.3b) was found to be porous, with a filament morphology (Fig.3c). The modified FTO substrate determined the

modification of nucleation and growth processes [21] which led to a different hematite morphology compared to that shown in the Fig.3a. Because the deposition was carried out following an electrochemical process, the hematite film has mainly grown into mesoporous TiO_2 structure which has a thickness of about 400 nm (Fig.3d).

The performance of the prepared hematite photoanodes was assessed based on photocurrent voltage (J-V) curves and electrochemical impedance spectra.

NiO is an oxygen evolution catalyst that we used it for modification of hematite surface in order to increase the holes transfer rate to water. In the Fig.4 are shown NiO nanoparticles (size ~ 25 nm) deposited on FTO substrate (deposition time 10 s). In the case of FTO/ $\alpha\text{-Fe}_2\text{O}_3$ substrate the deposition time was 1 s.

The experimentally measured potentials vs. Ag/AgCl were reported against the reversible hydrogen electrode (RHE): $E_{\text{RHE}} = E_{\text{Ag/AgCl}} + 0.059\text{pH} + E_{\text{Ag/AgCl}}^0$, with $E_{\text{Ag/AgCl}}^0 = 0.1976\text{V}$ at 25°C . The potentials were normalized to RHE because both the water oxidation potential and the hematite bands shift at the Nernstian rate of 59mV/pH [22].

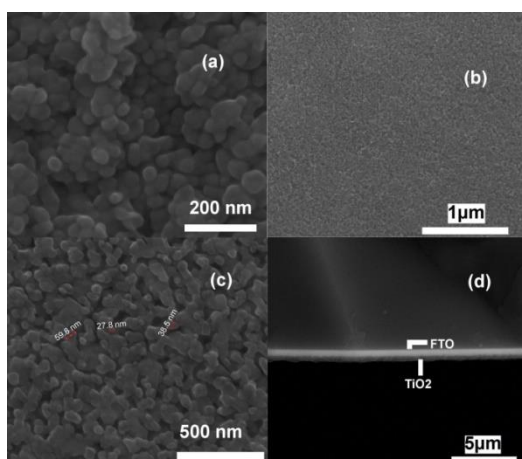


Fig.3. SEM images of: $\alpha\text{-Fe}_2\text{O}_3$ film deposited on FTO substrate (a), FTO/ mesoporous TiO_2 substrate (b), $\alpha\text{-Fe}_2\text{O}_3$ film deposited on FTO/mesoporous TiO_2 substrate (c); Cross-sectional SEM image of the mesoporous TiO_2 film deposited on FTO substrate (d).

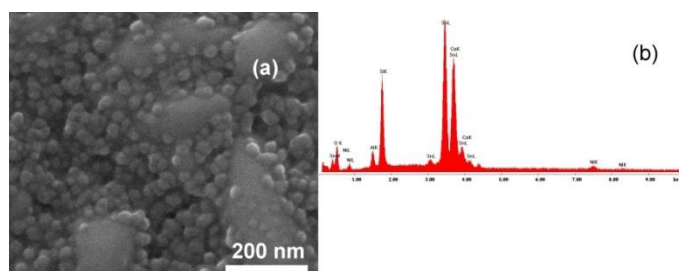


Fig.4. (a) SEM image of NiO nanoparticles deposited on FTO surface; (b) elemental analysis of the structure glass/FTO/NiO nanoparticles showed in the Fig.4a using an EDX measurement

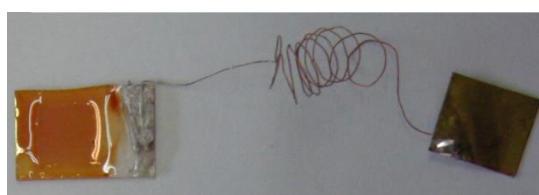


Fig. 5. The hematite photoanode with connecting cable

In the Fig.5 is shown the hematite photoanode ready for the photoelectrochemical measurements. The active surface of the photoanode was selected with epoxy resin.

Figs.6 A and B show the performance of variously-treated hematite samples by photocurrent density vs. applied potential (J-V) scans. It can be seen in Fig.6 A that modification of hematite surface with NiO nanoparticles causes a significant increase (curve a) in the photocurrent (0.63 mA) generated at 1.23V/RHE in comparison with the pristine hematite sample (curve b) which shows a photocurrent of 0.37 mA. The difference in the samples photoactivity is connected with the efficiency of transferring of the photogenerated carriers to the reactants from NaOH solution. On the other hand, α -Fe₂O₃/NiO photoanode is also more active as electrocatalyst than the pristine hematite (the dark current onset potential shifted to lower potentials).

Doping with metal elements such as Ti [23], Sn [24], Zr [25], Mn [26] is a major approach to enhance the electron mobility and consequently the photocurrent density. Recently, phosphorous has been successfully used as dopant to improve the electron mobility of hematite films [27]. We obtained phosphorous doped hematite film by impregnation of FeOOH film in 0.05M Na₂HPO₄ solution (pH 8) for 1 min [27] and then immediately annealed at 525^oC and 800^oC.

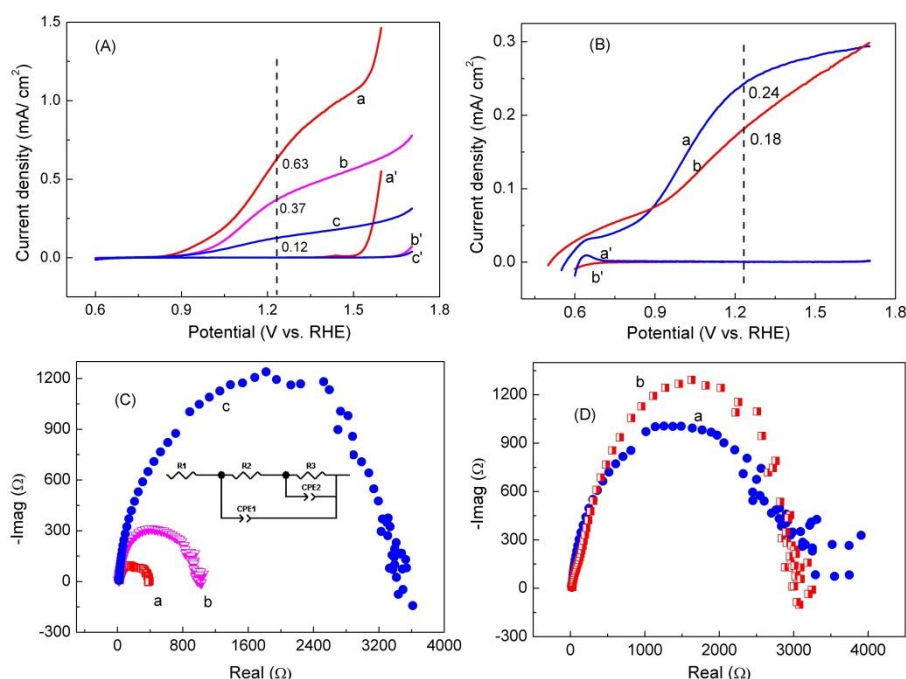


Fig.6. J-V characteristics obtained under simulated solar illumination (AM 1.5, 100mW cm⁻²) for (A) α -Fe₂O₃/NiO (a, red), α -Fe₂O₃ (b, magenta), phosphorous doped α -Fe₂O₃ (c, blue) and (B) TiO₂/phosphorous doped α -Fe₂O₃ (a, blue), TiO₂/ α -Fe₂O₃ (b, red) in 1M NaOH solution, pH=13.6. Dark curves are reported and are denoted a', b', c' and a', b' in the figures (A) and (B), respectively. Electrochemical impedance spectra collected at 1.23V/RHE, under illumination for (C) α -Fe₂O₃/NiO (a, red), α -Fe₂O₃ (b, magenta), phosphorous doped α -Fe₂O₃ (c, blue) and (D) TiO₂/phosphorous doped α -Fe₂O₃ (a, blue), TiO₂/ α -Fe₂O₃ (b, red).

Our results indicate that phosphorous doped hematite exhibits poor photoactivity as shown in Fig. 6A, curve c. This result could be connected with the influence of the pH on the phosphorous doped hematite synthesis [27].

In Fig.6 B are presented J-V characteristics of TiO₂/ phosphorous doped hematite (curve a) and TiO₂/hematite (curve b) recorded in 1M NaOH solution, in the dark and under illumination. Hematite was prepared by electrodeposition into the pores of the TiO₂ layer, in connection with FTO substrate. However, mesoporous TiO₂ underlayer with thickness of about 400 nm could

hinder the penetration of photoexcited electrons into FTO and result in a reduced photocurrent. The TiO₂/phosphorous doped hematite photoanode shows an enhanced photocurrent (curve a) at 1.23V compared to TiO₂/hematite photoanode (curve b). This improving in performance could be explained by formation of Fe₂TiO₅ thin layer at interface of hematite with TiO₂ and FePO₄ on surface which may improve charge separation and holes transfer [28]. On the other hand, for hematite photoanodes the onset of water oxidation photocurrent is usually not observed until 0.8-1.0 V/RHE [7]. In our case, TiO₂/hematite photoanodes show the onset of water oxidation photocurrent at about 0.6V/RHE.

Table 1 Parameters of the studied photoanodes obtained from impedance spectroscopy analysis.

Photoanode	R1 (Ωcm^2)	CPE1 (F/cm ²)	R2 (Ωcm^2)	CPE2 (F/cm ²)	R3 (Ωcm^2)
1. FTO/ α -Fe ₂ O ₃ / NiO	25.9	2.6x10 ⁻⁵	248.8	4.5x10 ⁻⁴	103.2
2. FTO/ α -Fe ₂ O ₃	19.3	3.2x10 ⁻⁴	755.1	1.3x10 ⁻⁵	199
3. FTO/P doped α -Fe ₂ O ₃	21.3	1.3 x10 ⁻⁵	2224	1x10 ⁻⁴	1127
4. FTO/TiO ₂ /P doped α -Fe ₂ O ₃	20.9	1.3 x10 ⁻⁵	2207	7.5x10 ⁻⁴	1719
5. FTO/TiO ₂ / α -Fe ₂ O ₃	23	1.8x10 ⁻⁵	661	5.9x10 ⁻⁶	2342

An additional evaluation of the hematite photoanodes was performed by impedance spectroscopy measurements. Figs.6 C and D show the Nyquist representations of the impedance spectra of the hematite photoanodes from the Table 1 under illumination AM 1.5, in 1M NaOH solution, at a potential of 1.23V/RHE. Fig.6 C also shows the equivalent circuit used to fit the impedance data.

In this model, R1 represents all series resistances in the photoelectrochemical cell, CPE1 represents the capacity of the region of spatial charge at the surface of the electrode, R2 represents resistance in the process of trapping of the holes by the surface states, the CPE2 capacity is correlated with the number of active centers from the surface states and R3 represents resistance in the charge transfer process through the interface. It can be seen from Table 1 that the value of R2 for photoanode 1 is about 3 and 9 times lower than the similar values for samples 2 and 3, respectively, at potential of 1.23V/RHE. This indicates that transfer of the photogenerated holes to surface states in FTO/ α -Fe₂O₃/NiO is easier than for bare hematite or phosphorous doped hematite. Can be also noted the small value of the R3 parameter for the sample 1, which indicates an easy charge transfer at the photoanode/electrolyte interface. Higher CPE2 capacity of the sample 1 indicates a larger number of holes trapped by the surface states. It has been demonstrated that water oxidation process takes place predominantly with the participation of holes trapped by the surface states [22]. In the case of sample 3, the high CPE2 capacity must be correlated with the high resistance value of the parameter R3. The use of the FTO/TiO₂ substrate led to the increase of the resistances R2 and R3. However, doping of phosphorus in hematite structure, in the sample 4 led to a lower value of the parameter R3 compared to similar value of R3 for sample 5, which is consistent with the obtained photocurrent (Fig.6 B).

5. Conclusions

We synthesised hematite films on FTO and TiO₂ modified FTO substrates using anodic electrodeposition and annealing processes. The mesoporous TiO₂ film was prepared on FTO substrate by spin coating a diluted TiO₂ paste. The hematite surface was modified with NiO nanoparticles and phosphorous was doped into hematite structure. The performance of the prepared hematite photoanodes was assessed based on photocurrent-voltage curves and electrochemical impedance spectra. The modification of hematite surface with NiO nanoparticles caused a significant increase in the photocurrent (0.63 mA) generated at 1.23V/RHE in comparison with the pristine hematite sample which showed a photocurrent of 0.37 mA. This

result was attributed to the increased efficiency of transferring of the photogenerated carriers to the reactants (modification of the hematite surface induced a significant decrease of the charge transfer resistance). In addition, the resistance of the process of holes trapping by the surface states decreased, which also favored water oxidation process.

The performance of hematite deposited on FTO/TiO₂ substrate is modest. However, TiO₂/hematite photoanodes show the onset of water oxidation photocurrent at about 0.6V/RHE, which represents a cathodic shift of 0.3V compared to that for hematite deposited on FTO substrate.

Phosphorous doped hematite showed a poor photoactivity, especially when the FTO substrate was used.

Acknowledgments

The financial support of Romanian Ministry of Education and Research (Core Program contract PN16-480102) is gratefully acknowledged.

References

- [1] K. Zhang, M. Ma, P. Li, D.H. Wang, J.H. Park, *Adv. Energy. Mater.* 2016, 1600602.
- [2] A. Marshall, B. Borresen, G. Hagen, M. Tsyppkin, R. Tunold, *Energy* **32**(4), 431 (2007).
- [3] A. Fujishima, K. Honda, *Nature* **238**, 37 (1972).
- [4] C. Santato, M. Odziemkowski, M. Ulmann, J. Augustynski, *J. Am. Chem. Soc.* **123**(43), 10639 (2001).
- [5] S.P. Berglund, D.W. Flaherty, N.T. Hahn, A.J. Bard, C.B. Mullins, *J. Phys. Chem. C* **115**(9), 3794 (2011).
- [6] A. Iwase, A. Kudo, *J. Mater. Chem.* **20**(35), 7536 (2010).
- [7] K. Sivula, F. Le Formal, M. Gratzel, *ChemSusChem* **4**(4), 432 (2011).
- [8] J. H. Kennedy, K. W. Fresse, Jr., **125**(5), 709 (1978).
- [9] M.P. Dare-Edwards, J.B. Goodenough, A. Hamnett, P.R. Trevellick, *J. Chem. Soc., Faraday Trans. 1*, **79**(9), 2027 (1983).
- [10] A. Kay, L. Cesar, M. Gratzel, *J. Am. Chem. Soc.* **128**(49), 15714 (2006).
- [11] I. Thomann, B. A. Pinaud, Z. Chen, B. M. Clemens, T. F. Jaramillo, M. L. Brongersma, *Nano Lett.* **11**(8), 3440 (2011).
- [12] R. F. G. Gardner, F. Sweett, D. W. Tanner, *J. Phys. Chem. Solids* **24**(10), 1183 (1963).
- [13] A. J. Cowan, C. J. Barnett, S. R. Pendlebury, M. Barroso, K. Sivula, M. Gratzel, J. R. Durrant, D. R. Klug, *J. Am. Chem. Soc.* **133**(26), 10134 (2011).
- [14] M. Gratzel, *Nature* **414**, 338 (2001).
- [15] J. Brillet, M. Cornuz, F. Le Formal, J. H. Yum, M. Gratzel, K. Sivula, *J. Mater. Res.* **25**(1), 17 (2010).
- [16] J. G. Yu, H. G. Yu, C. H. Ao, S. C. Lee, J. C. Yu, W. K. Ho, *Thin Solid Films* **496**(2), 273 (2006).
- [17] A. Garcia, G. C. Welch, E. L. Ratcliff, D. S. Ginley, G. C. Bazan, D. C. Olson, *Adv. Mater.* **24**(39), 5368 (2012).
- [18] R.L. Spray, K-S. Choi, *Chem. Mater.* **21**(15), 3701 (2009).
- [19] A.F. Gualtieri, P. Venturelli, *Am. Mineral.* **84**(5-6), 895 (1999).
- [20] K. Sivula, R. Zboril, F. Le Formal, R. Robert, A. Weidenkaff, J. Tucek, J. Frydrych, M. Gratzel, *J. Am. Chem. Soc.* **132**(21), 7436 (2010).
- [21] A. Annamalai, P.S. Shinde, A Subramanian, J.Y. Kim, J.H. Kim, S.H. Choi, J.S. Lee, J.S. Jang, *J. Mater. Chem. A* **3**(9), 5007 (2015).
- [22] B. Klar, S. Gimenez, F. Fabregat-Santiago, T. Hamann, J. Bisquert, *J. Am. Chem. Soc.* **134**(9), 4294 (2012).
- [23] J.A. Glasscock, P.R.F. Barnes, I.C. Plumb, N. Savvides, *J. Phys. Chem. C* **111**(44), 16477 (2007).

- [24] Y. Ling, G. Wang, D.A. Wheeler, J.Z. Zhang, Y. Li, *Nano Lett.* **11**(5), 2119 (2011).
- [25] P. Kumar, P. Sharma, R. Shrivastav, S. Dass, V.R. Satsangi, *Int. J. Hydrogen Energy* **36**(4), 2777 (2011).
- [26] Gurudayal, S.Y. Chiam, M.H. Kumar, P.S. Bassi, H.L. Seng, J. Barber, L.H. Wong, *ACS Appl. Mater. Interfaces* **6**(8), 5852 (2014).
- [27] Y. Zhang, S. Jiang, W. Song, P. Zhou, H. Ji, W. Ma, W. Hao, C. Chen, J. Zhao, *Energy Environ. Sci.*, **8**(4), 1231 (2015).
- [28] X. Lv, K. Nie, H. Lan, X. Li, Y. Li, X. Sun, J. Zhong, S-T. Lee, *Nano Energy* **32**, 526 (2017).